THE ASTROPHYSICAL JOURNAL, 342:364–378, 1989 July 1

THE GEOMETRY, COMPOSITION, AND MASS OF THE CRAB NEBULA

GORDON M. MACALPINE, STACY S. MCGAUGH, AND JOSEPH M. MAZZARELLA
University of Michigan, Ann Arbor

AND

ALAN UOMOTO
Johns Hopkins University
Received 1988 July 6; accepted 1988 December 9

ABSTRACT

Interference filter images and long-slit spectroscopy suggest that much of the brighter filamentary gas in the Crab Nebula is involved in large structures consisting of a nearly pure (~95% by mass) helium band or torus across the neutron star and bipolar, helium-rich lobes. Measured line intensities indicate that collisional contributions to observed exceptionally strong helium lines are insignificant. Therefore, the use of I(He I λ5876)/I(Hβ) to derive the helium to hydrogen abundance ratio is valid. The combined mass in the filaments (primarily helium) and the neutron star may be in the range of 6–9 $M_\odot$, suggesting that the supernova precursor may have initially contained 20–30 $M_\odot$.

The [Ni II] λ7378 emission implies an abundance enhancement by a factor of 55 compared with solar in the northern arch-shaped structure, assuming this line arises from collisional excitation in an equilibrium gas. In general, the strongest [Ni II] emission coincides with regions of relatively low helium abundance in the northeast part of the nebula, near the base of the jetlike protrusion. Other evidence is consistent with the idea that this overall situation may have resulted from interaction and mixing between an ambient interstellar cloud and material produced in the supernova, including nickel-rich gas from the central region.

Subject headings: nebulae: abundances — nebulae: Crab Nebula — nebulae: supernova remnants

I. INTRODUCTION

The Crab Nebula has a rich history of scientific discovery, and it reigns as the most carefully studied supernova remnant. Yet it is not well understood, and it deserves further attention because it presents unique opportunities for analyzing a supernova after the fact. The nebula is young (934 years old as observed) and it lies roughly 200 parsecs out of the galactic plane, so the expanding filamentary structure represents relatively undiluted debris from the explosive event. Furthermore, we see the filaments largely because of reprocessed synchrotron radiation, so the gas can be effectively analyzed by using numerical photoionization models. By studying the chemical composition, distribution, and dynamics of the emitting gas, it is reasonable to hope that we can better understand the characteristics of the precursor star along with certain details of the supernova explosion and associated nucleosynthesis.

Spectroscopy of numerous positions in the nebular filaments has been reported by Mayall (1937), Minkowski (1942), Woltjer (1958), Davidson (1978, 1979), Miller (1978), and Fesen and Kirshner (1982) for optical wavelengths, by Davidson *et al.* (1982) in the *IUE* satellite ultraviolet range, and by Dennefeld and Péquignot (1983) and Henry, MacAlpine, and Kirshner (1984) in the near-infrared. Photoionization model analyses for these data have been carried out by Williams (1967), Davidson (1973), Henry and MacAlpine (1982, hereafter HM) and Péquignot and Dennefeld (1983). It was confirmed that the helium mass fraction is unusually high and spatially variable, assuming the helium and hydrogen lines arise from recombination. The deduced abundances of carbon, nitrogen, oxygen, and neon have brought about consideration of a progenitor mass in the 9–10 $M_\odot$ range (e.g., Nomoto 1985), although it is difficult to account for the element fractions in a consistent fashion (see Davidson and Fesen 1985 or Henry 1986). Whereas the carbon abundance initially estimated from the data of Davidson *et al.* (1982) seems low compared with what would be expected following some postulated helium shell burning, Eastman *et al.* (1985) have demonstrated that the estimate should be revised upward when the transfer of He II Lyα radiation is properly taken into account. It was found that the usual assumption of on-the-spot absorption for these 3 Ry photons results in excess energy being radiated by the ultraviolet carbon lines, thereby decreasing the modeled carbon abundance. The *most* anomalous nebular emission appears to be [Ni II] λ7378, which shows an exceptionally high relative intensity at some filament positions (e.g., Miller 1978; Fesen and Kirshner 1982; Henry, MacAlpine, and Kirshner 1984). Element abundances in the Crab Nebula have recently been discussed by Henry (1986), and a comprehensive review may be found in Davidson and Fesen (1985).

The mass of gas in the filaments was estimated by HM to be of order 1.5 $M_\odot$. Allowing for 1.5–2 $M_\odot$ in the neutron star suggests that roughly 6 $M_\odot$ from the progenitor are not visible. Searches for this material, which has been postulated to exist in a circumnebular shell, have been carried out at optical (e.g., Murdin and Clark 1981), radio (e.g., Wilson and Weiler 1982; Velusamy 1985), and X-ray (e.g., Schattenberg *et al.* 1980) wavelengths. Its existence has not been convincingly demonstrated.

Using CCD images obtained through interference filters, the He I λ5876/Hβ emission ratio has been mapped for the filamentary structure by Uomoto, MacAlpine, and Henry (1985) and Uomoto and MacAlpine (1987, hereafter UM). Assuming the above lines arise from recombination, model calculations indicate that the helium mass fraction may vary from more than 90% in a broken east-west band (high-helium band or HHeB) across the neutron star to less than 38% in the northeast region (low-helium region or LHeR), near the base of the

feature sometimes referred to as the "jet" or "stem" (see, e.g., van den Bergh 1970; Gull and Fesen 1982). Davidson (1987) recently employed a raster scanning technique to develop a representative integrated spectrum for the Crab Nebula as a whole, thereby deriving an estimate of about 70% for the global helium mass fraction.

This paper reports several kinds of new observations. Images through interference filters centered on [S II] and [Ni II] emission lines show that [Ni II] λ7378 is not distributed like other lines; rather, the emission arises primarily from a few filaments or areas, the most prominent of which appear to coincide with the LHeR. In addition, long-slit spectra have been obtained at a number of positions in order further to investigate geometrical or dynamical structures and abundance anomalies suggested in the He I λ5876/Hβ image reported by UM. We confirm strong spatial variations in emission features, an exceptionally high helium mass fraction in the HHeB, and bipolar nebular structure. Finally, long-slit "drift scans" yield spectra which are reasonably consistent with Davidson's (1987) line measurements for the nebula as a whole. However, we suggest that the total mass of emitting gas (largely helium) may be several times greater than previously estimated. Our data also support Davidson's contention that the [O III] line equivalent widths are increasing with time.

The line-emission images are presented in § II, followed by the long-slit spectroscopic observations along with a discussion of nebular geometry, dynamics, and element abundances in § III. The drift-scan data are reported in § IV, and § V contains a summary of results.

II. INTERFERENCE FILTER IMAGES

Images of the Crab Nebula were obtained through ~100 Å bandpass interference filters on 1988 February 12/13 and 16/17. We used an RCA CCD in direct mode on the McGraw-Hill 1.3 m telescope at the Michigan-Dartmouth-MIT Observatory. Figures 1 and 2 show the central 3′ × 3′ region through

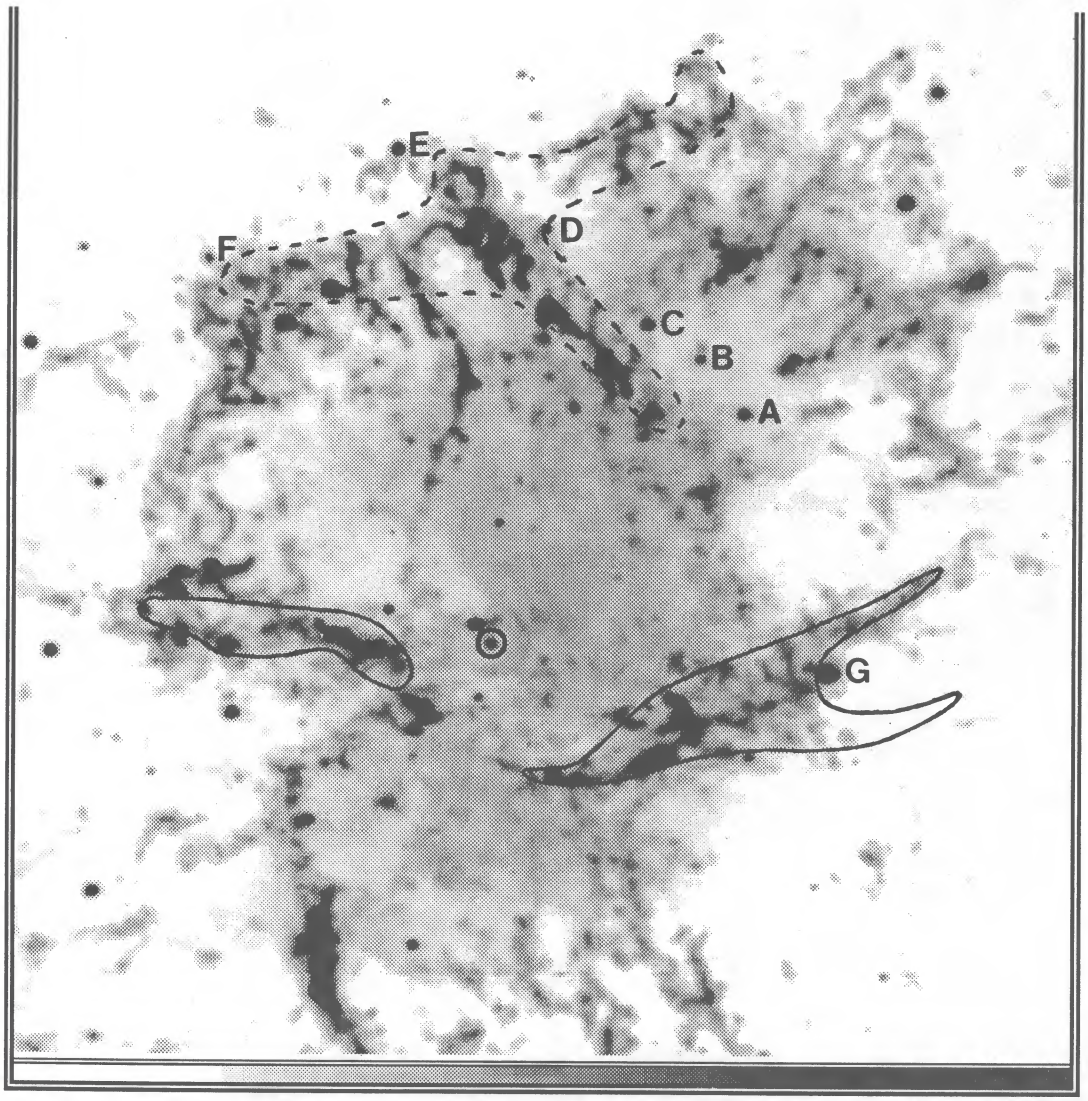

FIG. 1.—Crab Nebula CCD image obtained through an interference filter centered on [S II] $\lambda\lambda$6716, 6731 emission. North is up, east is to the left, and the field is approximately 3′ × 3′. The solid line roughly borders the HHeB from Fig. 3 of UM, and the dashed line roughly borders the LHeR. The pulsar is circled, and letters label reference stars for spectroscopic slit positions (*see text*).

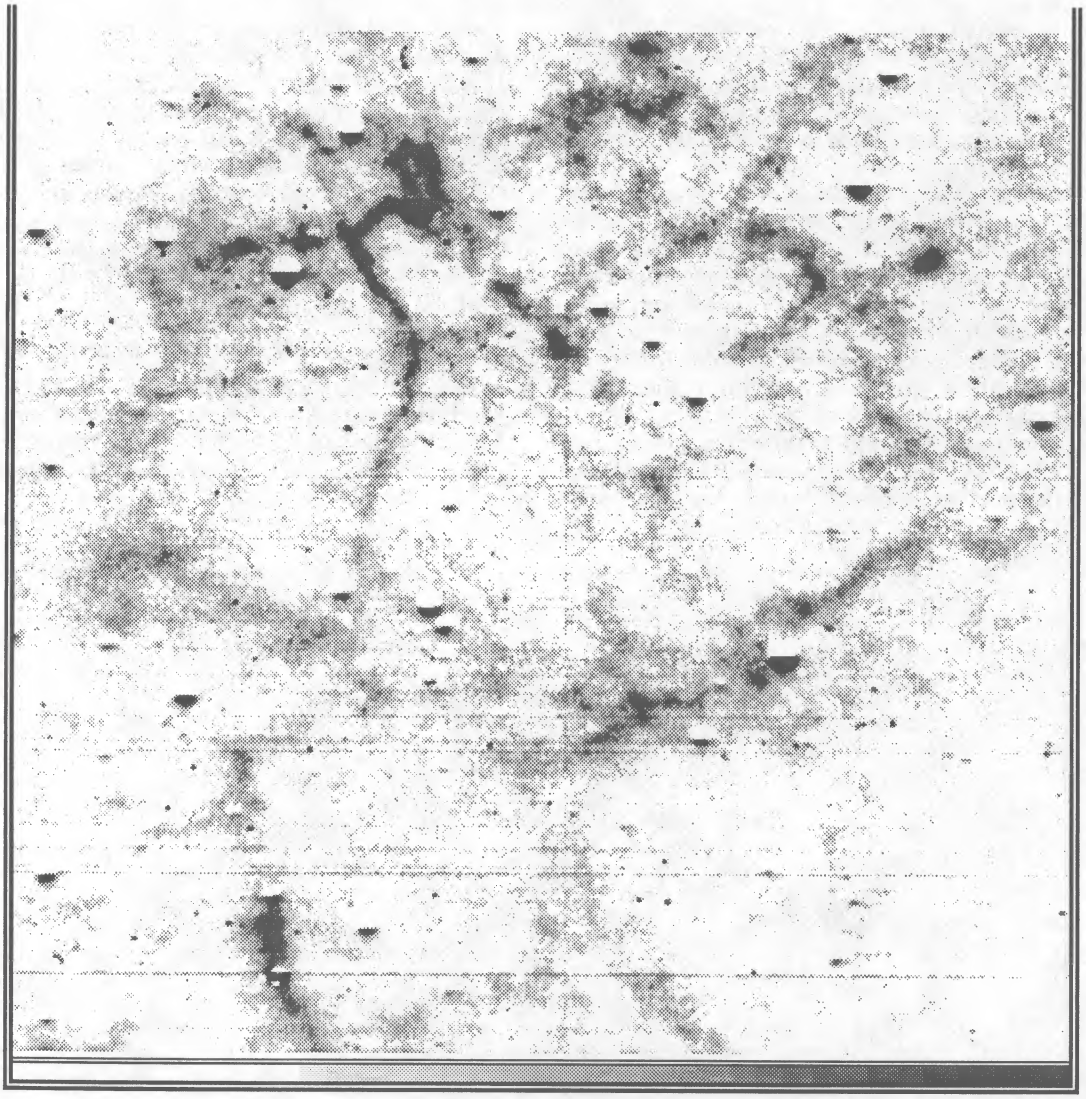

FIG. 2.—Crab Nebula CCD image obtained through an interference filter centered on [Ni II] λ7378 emission. North is up, east is to the left, and the field is roughly 3′ × 3′. A continuum image has been subtracted.

filters roughly centered on the [S II] λλ6716, 6731 and [Ni II] λ7378 emission, respectively. For the latter case, an image taken through a nearby continuum filter has been subtracted (leaving partial star residuals because of imperfect frame alignment). The frames have north up, east to the left, and a scale of 0.62″ per pixel.

For reference purposes, in Figure 1 the pulsar is circled, prominent parts of the HHeB are enclosed by solid lines, and the LHeR is outlined by a dashed border. The lettered stars refer to positions for spectroscopy, as discussed in the next section.

The [S II] emission stands out in the brighter parts of the filamentary structure, including the HHeB, some of the LHeR, and the elongated feature to the southeast which is often referred to as Miller's position 1. The [Ni II] line can also be seen in these three bright regions, but it is strongest in the LHeR, primarily in the arch-shaped structure and nearby knots where [S II] is not particularly prominent. If [S II] is a tracer of low-ionization emission regions, then [Ni II] must be exceptionally strong from the relatively helium-poor gas. As indicated in the next section, almost certainly the helium lines and plausibly the nickel lines reflect actual abundances, and we shall discuss a possible explanation for their apparent anti-correlation as a function of position in the Crab Nebula.

III. LONG-SLIT SPECTROSCOPY

a) Observations

Spectra of the Crab Nebula were obtained on 1987 January 3/4 and 4/5 with the McGraw-Hill 1.3 m telescope. We used the Mark III spectrograph with a 135 mm camera, a 300 lines per mm grism blazed at 5000 Å, and an RCA CCD as the detector. The projected slit size was 2.3″ × 9′, resulting in a reciprocal dispersion of about 7 Å per pixel, wavelength coverage of roughly 4000 Å to 7400 Å, and good sky coverage beyond the extent of the nebula. For each observation, the slit was carefully positioned on one of stars A through E in Figure 1, with the long axis oriented north-south.

Additional spectra were observed on 1987 October 14/15, 16/17, and 17/18 using the same telescope and spectrograph,

but with a Thomson CCD as the detector. The reciprocal dispersion was about 5 Å per pixel. With the same grism and slit described above, a 4000 Å to 7400 Å spectrum was obtained for the slit oriented east-west through star G. Also, using a 300 lines per mm grism blazed at 8000 Å along with an RG610 filter, 7200 Å to 9900 Å spectra were obtained for the star A, B, E, and G positions.

The Hiltner 2.4 m telescope was used on 1988 March 5/6 with the Mark III spectrograph and Thomson CCD to obtain a 4100 Å to 7500 Å spectrum with the slit passing through both stars D and F. In this case, the projected slit width was 1".3 and the reciprocal dispersion was about 5 Å per pixel.

Selected, fully reduced (using IRAF software) two-dimensional spectra are shown as negative reproductions in Figures 3, 4, and 5. Cosmic-ray spots have been removed where possible, although they are still evident in some of the spectra, which had typical total exposure times around an hour.

b) Geometrical and Dynamical Implications

Most of the spectra show reasonably well defined velocity ellipses for the lines, indicating that the brighter filaments are moving with coordinated radial velocities for the most part. Also, some relatively stationary material is apparent, for example, the patch seen within the velocity ellipses for the star A slit position.

Shapes or distortions of the velocity ellipses are particularly noteworthy for comparison with Figure 3 of UM, which is suggestive of bipolar "bubbles" in the filamentary structure above and below the HHeB. For the north-south slit orientations, the ellipses tend to be wasp-waisted, with a central pinched appearance, consistent with the expansion being somewhat constrained in the vicinity of the HHeB. For example, the star B slit position velocity ellipses for He I λ5876 and [O I] $\lambda\lambda$6300, 6364 are shown enlarged in Figure 6.

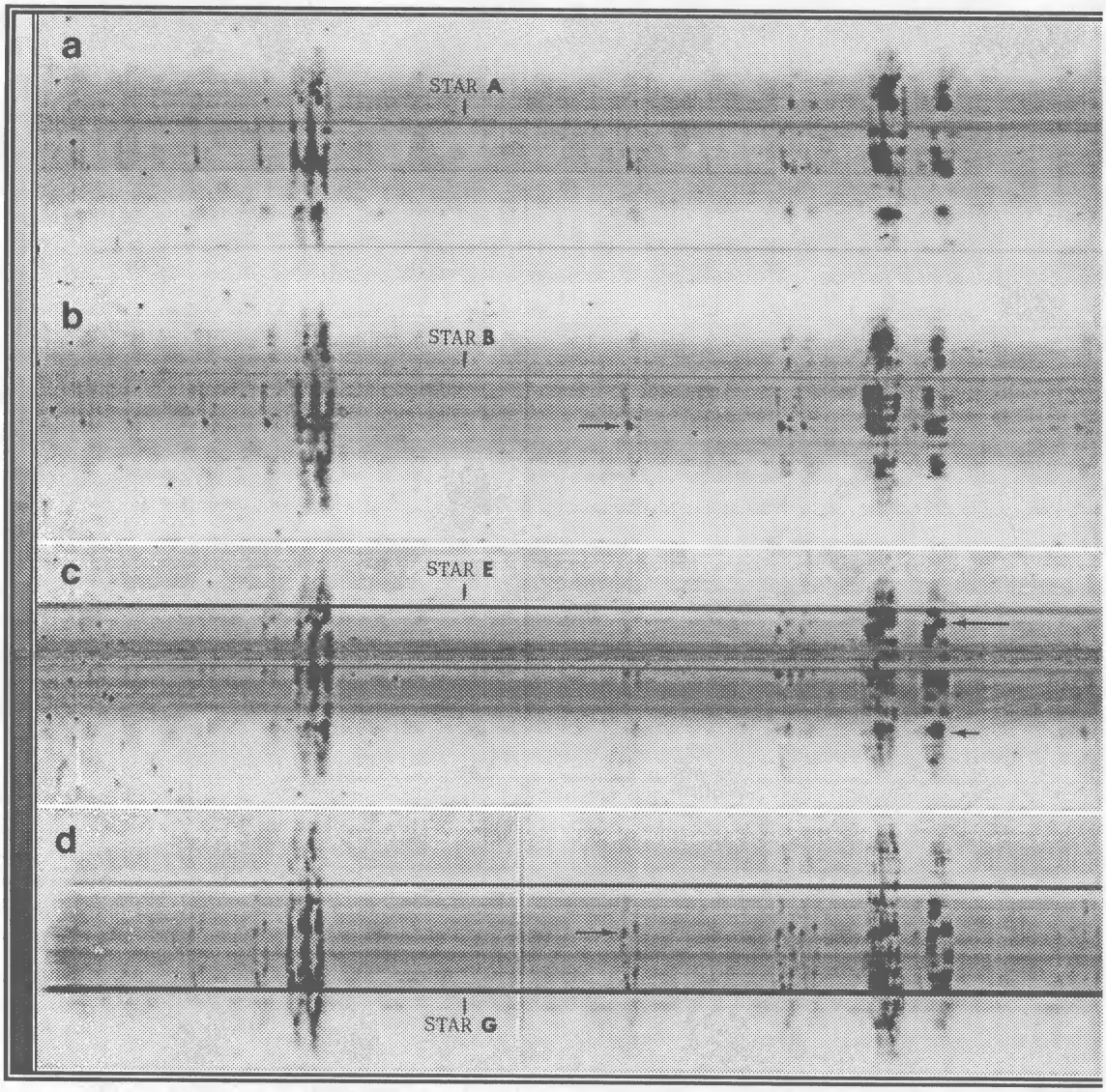

FIG. 3.—Two-dimensional spectra for: (*a*) the north-south slit through star A of Fig. 1, (*b*) the north-south slit through star B, (*c*) the north-south slit through star E, and (d) the east-west slit through star G. The illustrated wavelength range is roughly 4200 Å–7200 Å. Arrows mark positions for which one-dimensional spectra were extracted and measured. Line identifications may be found in the one-dimensional spectra.

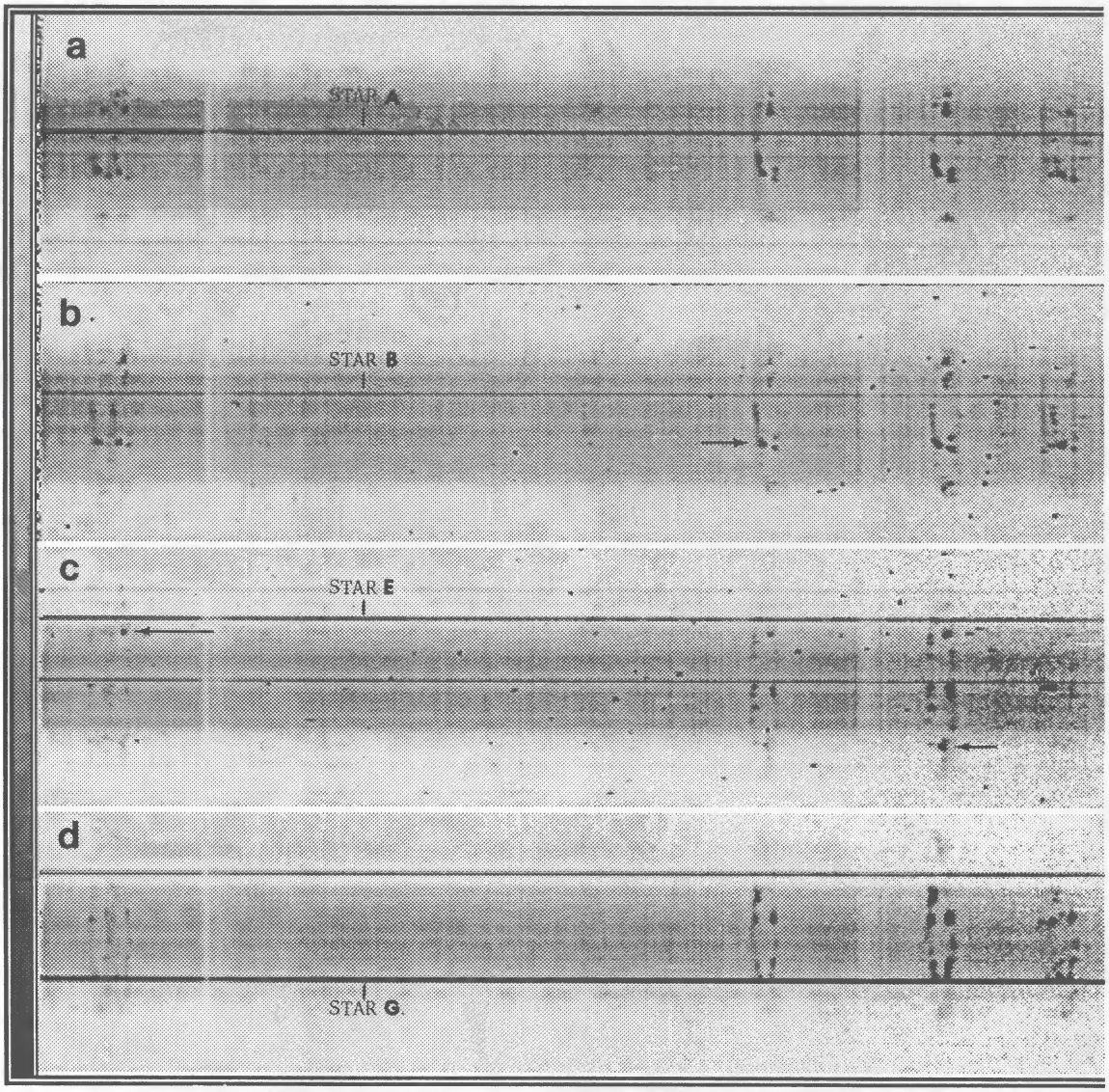

FIG. 4.—Two-dimensional spectra for: (*a*) the north-south slit through star A of Fig. 1, (*b*) the north-south slit through star B, (*c*) the north-south slit through star E, and (*d*) the east-west slit through star G. The illustrated wavelength range is roughly 7200 Å–9900 Å. Arrows mark positions for which one-dimensional spectra were extracted and measured. Line identifications may be found in the one-dimensional spectra.

Minimum measured expansion velocities at the HHeB are -400 and $+600$ km s^{-1}, while the velocities north or south of the HHeB reach -1120 and $+1680$ km s^{-1} or -950 and $+1190$ km s^{-1}, respectively. Uncertainties in these measurements, obtained from line centroids, are of order 60 km s^{-1}.

Distorted velocity ellipses in the Crab Nebula were first noted by Mayall (1937), who remarked that they are "probably related to the fact that the Crab Nebula noticeably departs from the ideal case of a spherically symmetrical expanding mass of gas." To our knowledge, their significance has not received further attention. Clarke *et al.* (1983), who obtained numerous long-slit spectra, did not detect pinched velocity ellipses because their slits were all oriented east-west. This was also the case for our star G slit position, which resulted in symmetrically smooth velocity ellipses with maximum measured velocities of -1500 and $+900$ km s^{-1} for the brighter HHeB filaments. Our observations, as well as the overall velocity maps developed by Clark *et al.*, provide support for the existence of large, bubble-like bipolar structures to the north and south of the HHeB. The HHeB may take the form of a ring or torus in order to constrain the expansion.

c) *Physical Conditions and Chemical Abundances*

The two-dimensional spectra in Figure 3 demonstrate that exceptionally strong He I emission is confined to the HHeB, which is also bright in other lines. On the other hand, Figure 4 confirms that the [Ni II] λ7378 line tends to be strongest in the LHeR. Finally, we note that [C I] $\lambda\lambda$9823, 9850 emission, which is known to be anomalously high at some locations (Dennefeld and Andrillat 1981; Henry, MacAlpine, and Kirshner 1984), appears to be more intense in the HHeB than in the LHeR. One-dimensional spectral extractions for selected positions are shown in Figures 7, 8, 9, and 10.

The spectra of Figures 7*a* and 9 come from the HHeB at the star B slit position (marked with an arrow in Fig. 3*b*) and from the star G east-west slit location marked with an arrow in Figure 3*d*, respectively. We shall use them to demonstrate that collisional contributions to the helium lines are probably insig-

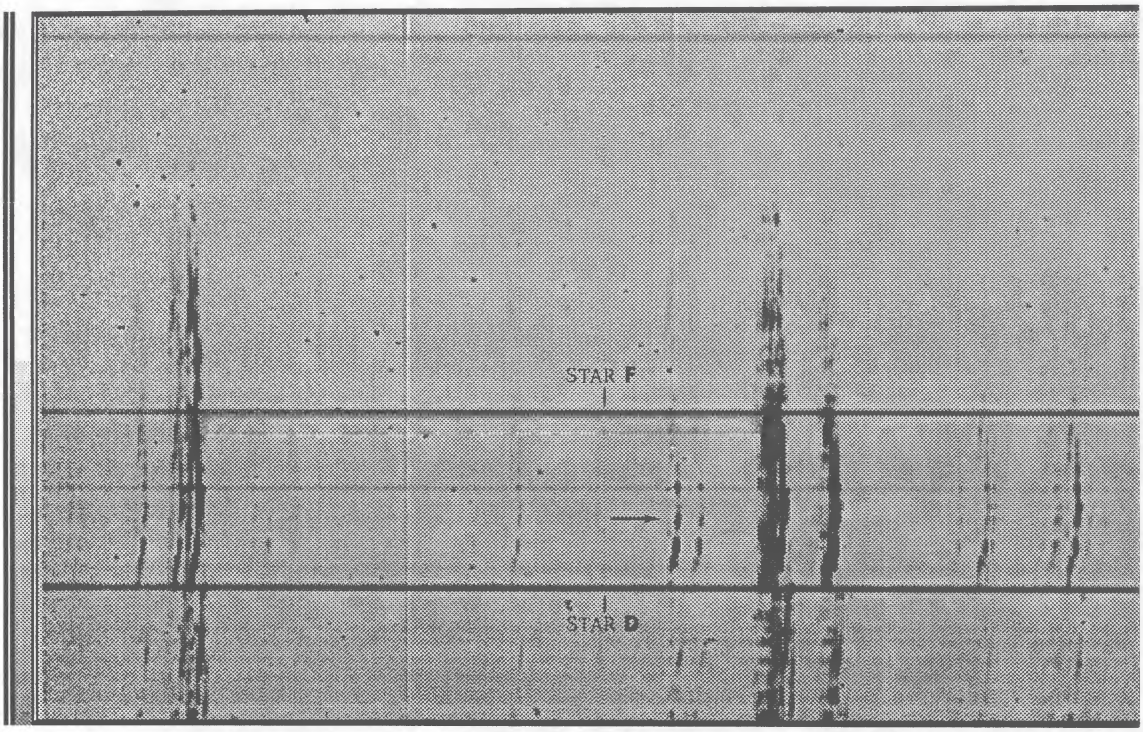

FIG. 5.—Two-dimensional 4100 Å–7500 Å spectrum for the slit positioned through stars D and F in Fig. 1. The arrow marks the position for which a one-dimensional extracted spectrum (with line identifications) is illustrated in Fig. 10.

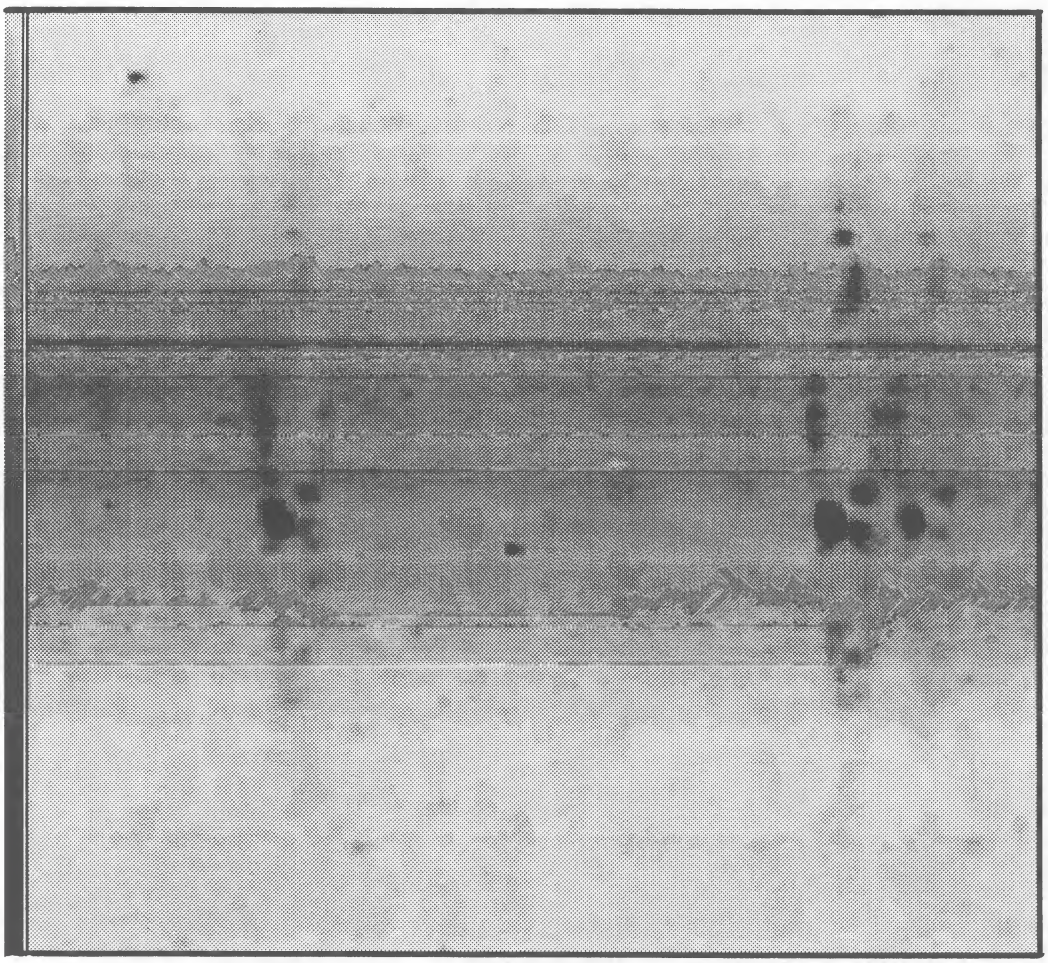

FIG. 6.—Enlargement of He I λ5876 and [O I] λλ6300, 6364 velocity ellipses from Fig. 3*b*

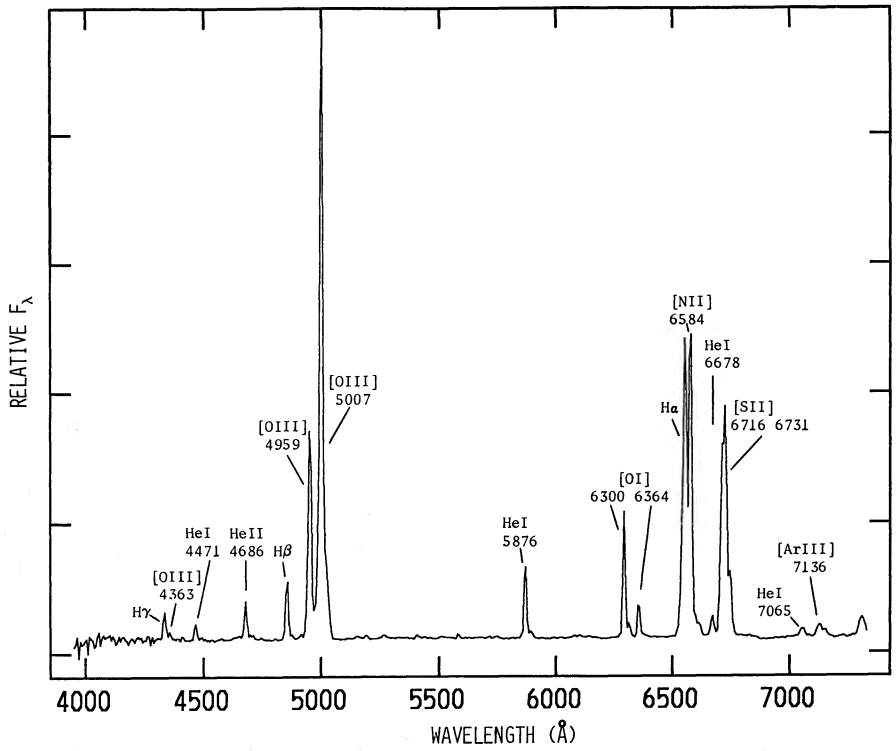

FIG. 7*a*

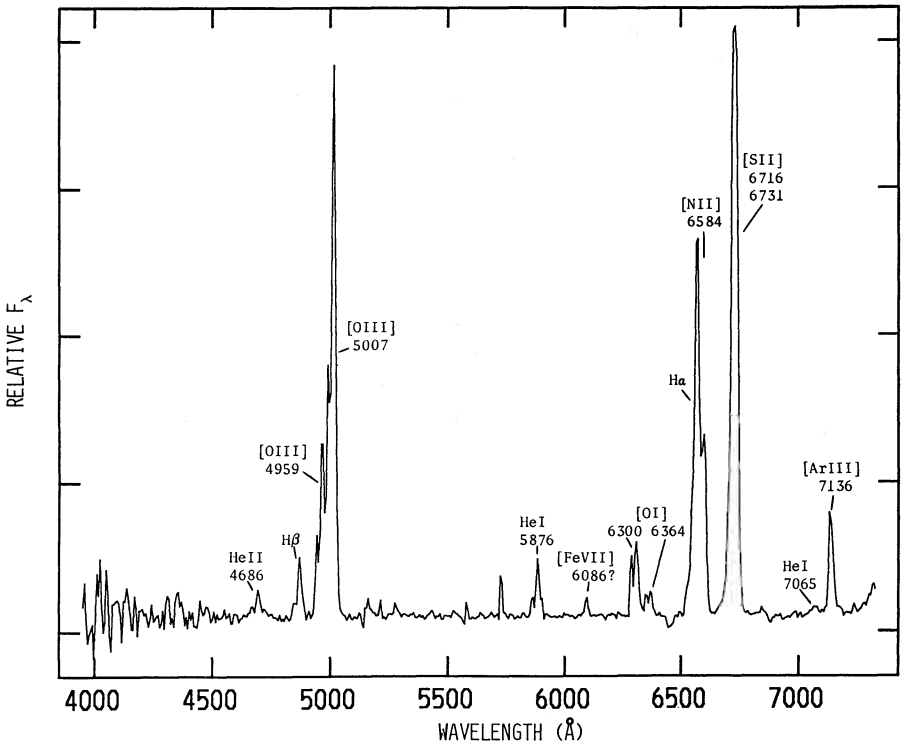

FIG. 7*b*

FIG. 7.—One-dimensional spectral extractions for : (*a*) the HHeB position marked with an arrow in Fig. 3*b*, (*b*) the position marked with a short arrow in Fig. 3*c*, and (*c*) the LHeR position marked with a long arrow in Fig. 3*c*.

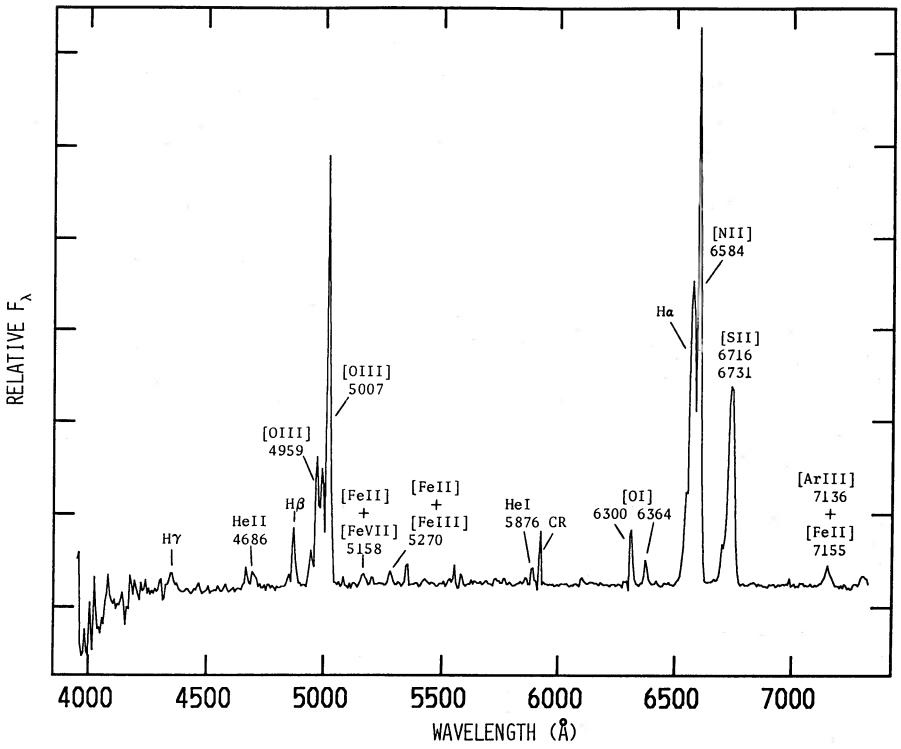

FIG. 7c

nificant. The measured He I λ5876/Hβ ratio, corrected for differential extinction using $E(B-V) = 0.47$ magnitude (see Davidson and Fesen 1985 and references therein), is around 1.0 (see Table 1). In order to convert this line intensity ratio to a helium to hydrogen number density ratio, N(He)/N(H), it is common practice to consider only recombination processes for the relevant emission, an assumption which must be checked for such strong helium lines.

Enhancement of He I λ5876 via $2\,^3P$–$3\,^3D$ electron collisional excitation, pointed out by MacAlpine (1976) as being important in some Seyfert galaxies, is not expected to be significant for densities characterizing the Crab Nebula filaments. On the other hand, collisions directly out of the metastable $2\,^3S$ level may affect the data. Relevant rate coefficients tabulated by Feldman and MacAlpine (1978), as derived from the eikonal computations of Flannery and McCann (1975), and by Clegg (1987), as derived from the 19-state close-coupled calculations of Berrington and Kingston (1987), are about a factor of 1.7 below the rate coefficients reported by Ferland (1986), as derived from the 11-state calculations of Berrington *et al.* (1985). We adopt the collision rate coefficients listed by Clegg as being the most reliable because they are based upon the most complete quantal calculations.

Relative measured line fluxes and reddening corrected [$E(B-V) = 0.47$] intensities from the spectra of Figures 7*a* and 9 (blue line components only) are given in columns (2), (3), (4), and (5) of Table 1. Typical measurement uncertainties are estimated to be 15% or less, whereas a colon following an entry indicates the error may be as high as 25%. Also, the normalization between blue and red spectra could conceivably be off by as much as 25% due to small-scale spatial variations in the nebula, and this may affect comparisons of lines from the two wavelength ranges.

The [S II] $\lambda\lambda$6716/6731 ratios from data in columns (3) and (5) of Table 1 suggest an electron density of about 1–2 $\times$ 10^3 cm^{-3}, and the [O III] $\lambda\lambda$4363/5007 ratio from column (3) yields an electron temperature around 12,000 K. For these conditions, Table 3 of Clegg (1987) indicates that relative collisional enhancement factors (compared with recombination for each line) would be about 0.04, 0.1, 0.05, and 1.0 for He I $\lambda\lambda$4471, 5876, 6678, and 7065, respectively. Our Table 2 contains reddening corrected helium line ratios, along with their expected case B recombination values (Osterbrock 1974) and the ratios to be expected if there were a 10% collisional enhancement of He I λ5876. The data, particularly $I(\lambda 6678)/I(\lambda 7065)$, appear to rule out collisional contributions to He I λ5876 at or above the 10% level.

If gas elsewhere in the Crab has higher temperature or density, collisions could become important, but λ7065 would always be enhanced substantially more than other lines so the effects should be easily recognized. Whereas we have not found evidence for helium line collisional excitation in most of our data, we did find one spot which apparently shows unusually strong λ7065 emission and this will be investigated further. Another way of increasing λ7065 emission involves scattering and fluorescence of λ3889 photons. Although optical depths in the filaments would not normally be expected to support this process, it will also be considered.

Having demonstrated that the helium lines arise primarily from recombination processes, we still must use detailed model calculations to convert I(He I λ5876)/I(Hβ) $\gtrsim$ 0.5 into N(He)/N(H), as noted by HM. This line intensity ratio in Crab Nebula filaments would be expected to scale approximately as

$$\frac{I(\text{He I } \lambda 5876)}{I(\text{H}\beta)} = \int_{\nu_2}^{\nu_4} \frac{N(\text{He}^0)a_\nu(\text{He}^0)}{N(\text{He}^0)a_\nu(\text{He}^0) + N(\text{H}^0)a_\nu(\text{H}^0)} \frac{F_\nu}{h\nu}\, d\nu \Big/ \int_{\nu_1}^{\infty} \frac{F_\nu}{h\nu}\, d\nu\,, \qquad (1)$$

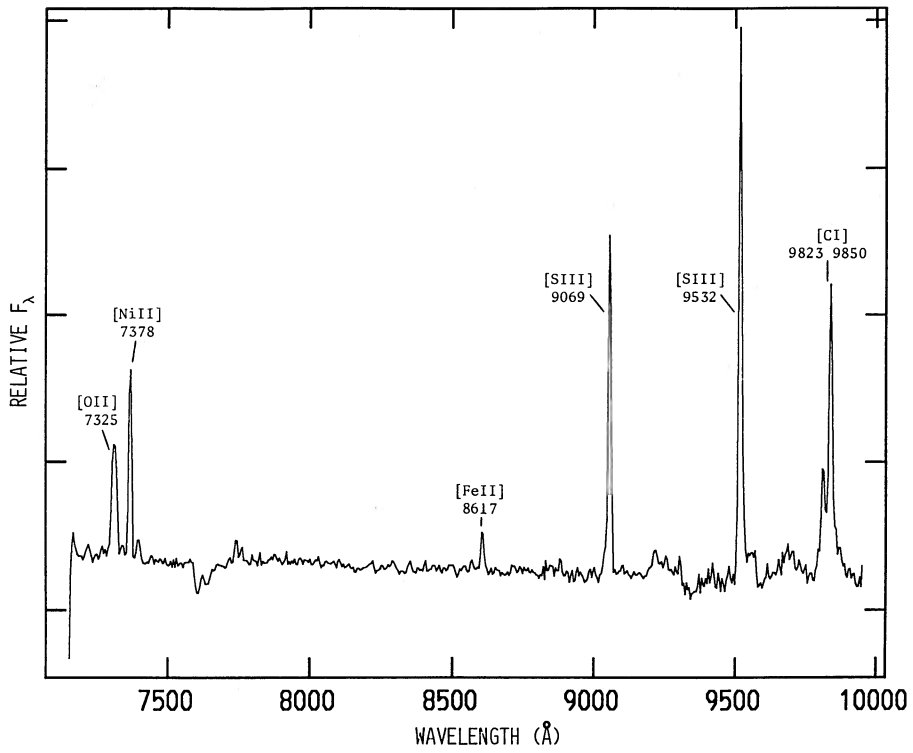

FIG. 8*a*

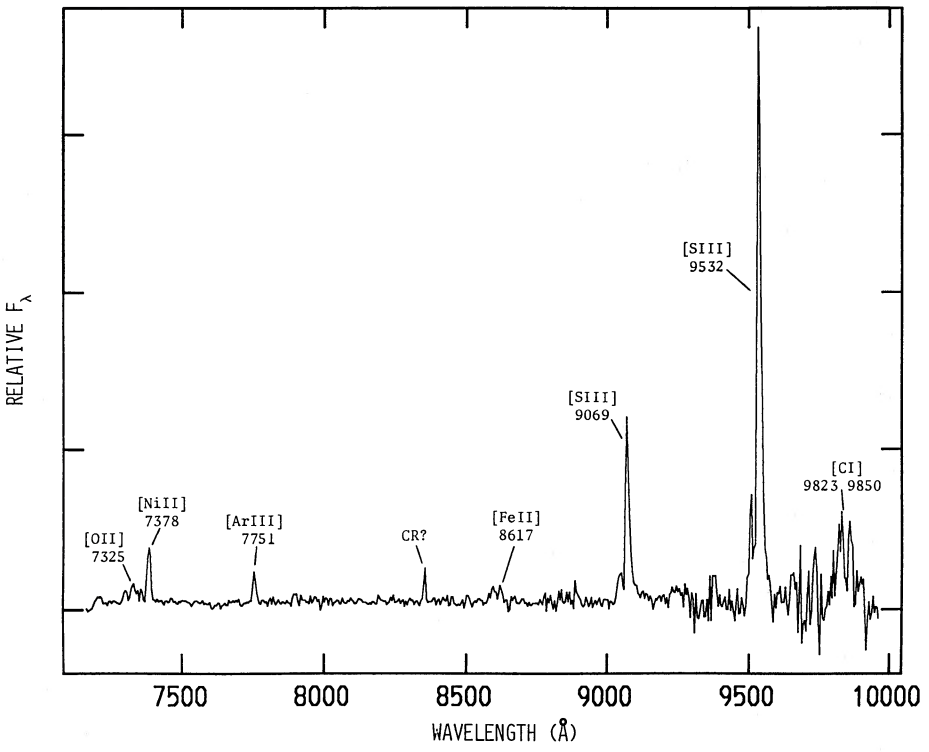

FIG. 8*b*

FIG. 8.—One-dimensional spectral extractions for: (*a*) the HHeB position marked with an arrow in Fig. 4*b*, (*b*) the position marked with a short arrow in Fig. 4*c*, and (*c*) the LHeR position marked with a long arrow in Fig. 4*c*.

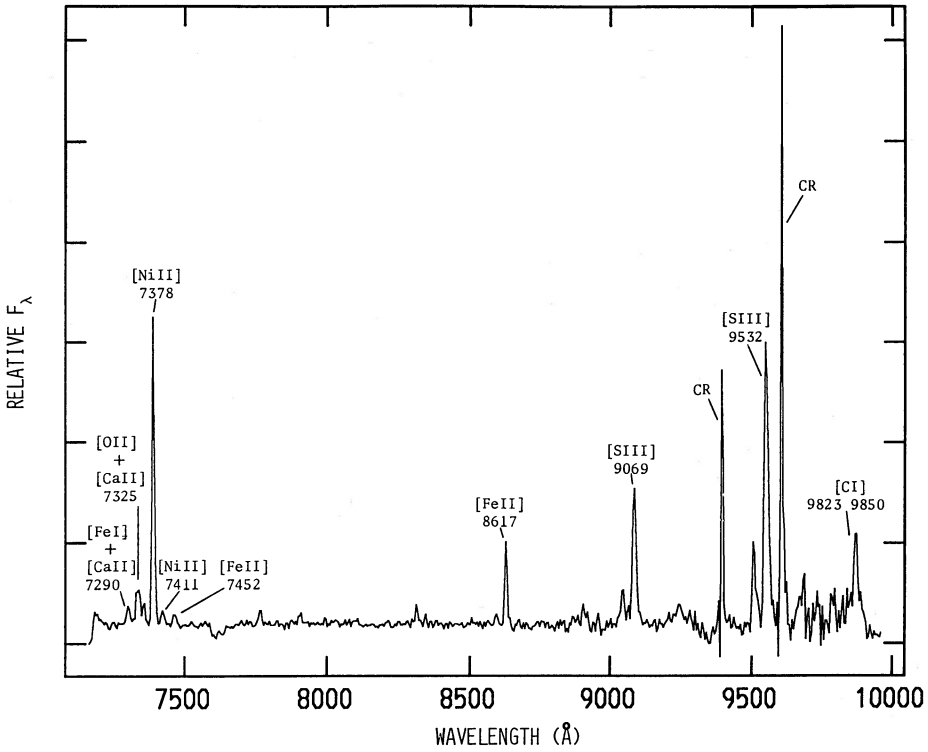

FIG. 8c

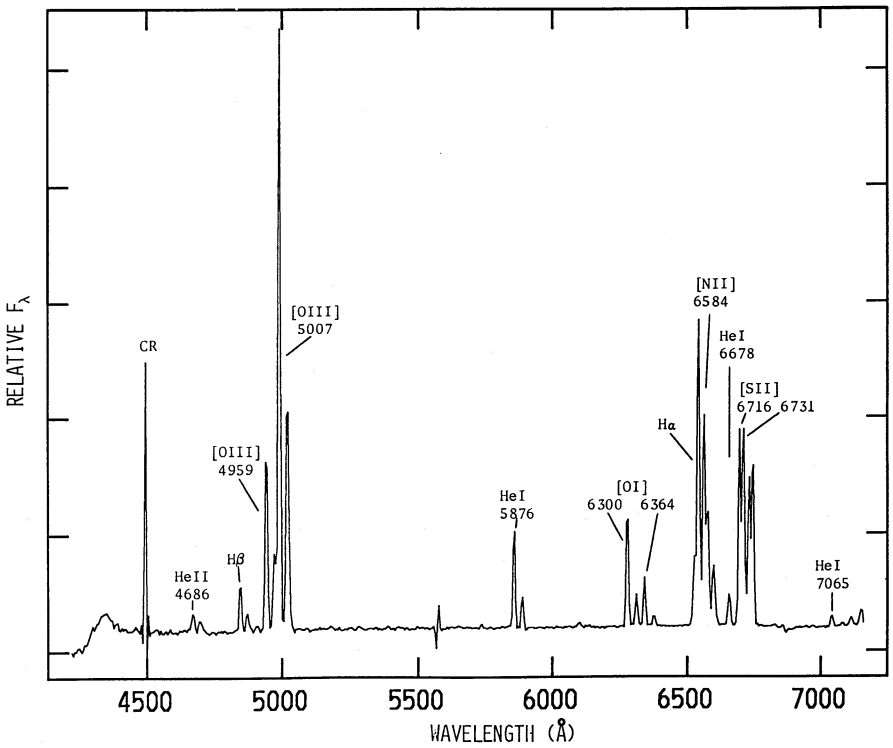

FIG. 9.—One-dimensional spectral extraction for the HHeB position marked with an arrow in Fig. 3d

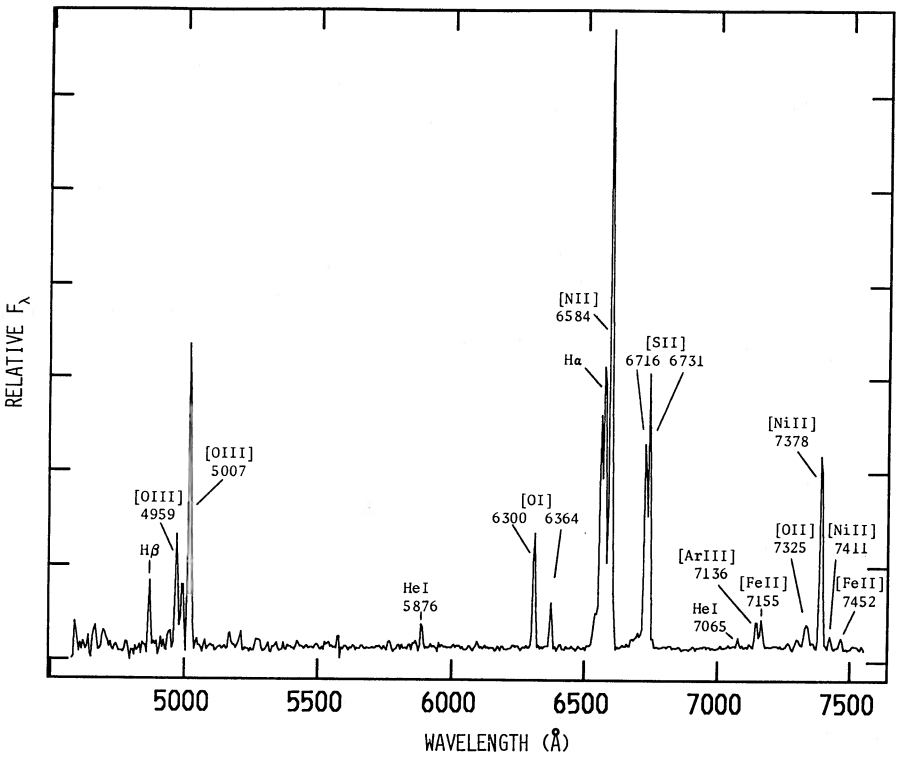

FIG. 10.—One-dimensional spectral extraction for the LHeR "arch" position marked with an arrow in Fig. 5

TABLE 1

RELATIVE MEASURED FLUXES AND REDDENING-CORRECTED INTENSITIES
[$I(H\beta) = 1.0$; $E(B-V) = 0.47$]

	NEBULA POSITIONS									
LINE ID (1)	F^a (2)	I^a (3)	F^b (4)	I^b (5)	F^c (6)	I^c (7)	F^d (8)	I^d (9)	F^e (10)	I^e (11)
Hγ 4340	0.44	0.54					0.6:	0.7:		
[O III] 4363	0.11	0.14								
He I 4471	0.26	0.30								
He II 4686	0.53	0.57	0.53	0.57	0.5:	0.6:	0.37	0.39		
Hβ 4861	1.00	1.00	1.00	1.00	1.00	1.00	1.00	1.00	1.00	1.00
[O III] 5007	12.2	11.5	11.6	11.0	8.50	8.03	6.90	6.52	5.89	5.56
He I 5876	1.21	0.86	2.03	1.43	0.90	0.63	0.25	0.18	0.41	0.29
[O I] 6300	1.88	1.19	2.45	1.56	1.15	0.73	0.91	0.58	1.90	1.21
Hα 6563	5.45	3.26	6.67	3.99	6.96	4.16	4.38	2.62	4.90	2.93
[N II] 6584	5.76	3.43	4.50	2.68	3.46	2.06	9.71	5.78	12.5	7.41
He I 6678	0.40	0.23	0.68	0.40						
[S II] 6716	3.33	1.93	3.77	2.18	17.1	9.88	7.19	4.16	3.53	2.04
[S II] 6731	4.09	2.36	4.15	2.40					4.30	2.48
He I 7065	0.21	0.11	0.28	0.15	0.25:	0.13:			0.14	0.08
[Ar III] 7136	0.35	0.19			2.00	1.07	0.60	0.32	0.54	0.29
[O II] 7325	0.48	0.25			0.31	0.16	0.68	0.36	0.72	0.38
[Ni II] 7378	0.49	0.25			0.70	0.36	3.28	1.69	3.78	1.95
[Fe II] 8617	0.11	0.05			0.20	0.09	0.88	0.37		
[S III] 9532	1.58	0.59			7.62	2.84	5.29	1.97		
[C I] 9823 + 9850	1.61	0.59					1.9:	0.7:		

[a] HHeB position in star B north-south slit.
[b] Position marked with an arrow in Fig. 3*d*.
[c] Position marked with a short arrow in Figs. 3*c* and 4*c*.
[d] Position marked with a long arrow in Figs. 3*c* and 4*c*.
[e] Position marked with an arrow in Fig. 5.

TABLE 2

HELIUM LINE RATIOS

Ratio	Star B HHeB Position	Star G HHeB Position	Case B Recombination	With Collisions (10% of λ5876)
5876/4471.....	2.86	...	2.76	2.92
6678/7065.....	2.09	2.62	2.40	1.26
5876/6678.....	3.71	3.60	3.49	3.66
5876/7065.....	7.82	9.43	8.41	4.63

where F_ν is the flux density of ionizing radiation, ν_1, ν_2, and ν_4 are ionization threshold frequencies of H^0, He^0, and He^+, respectively, and a_ν represents photoionization cross sections at frequency ν. As shown in Figure 1 of HM, there is approximately a linear relationship between I(He I λ5876)/I(Hβ) and N(He)/N(H) up to a value of about 0.5 for both quantities. As the helium abundance is further increased, the bracketed opacity ratio in expression (1) above approaches unity, so the line flux ratio becomes less sensitive. The most extreme case illustrated by HM indicates that I(He I λ5876)/I(Hβ) of 0.625 corresponds with N(He)/N(H) of about 2. Extrapolation to a line ratio of 1.0 suggests that some of the Crab Nebula HHeB gas contains 95% helium by mass fraction.

Next we consider the nickel and iron line measurements for the HHeB at the star B slit position. Using computations in Henry, MacAlpine, and Kirshner (1984) and scaling appropriately, we find that the [S II] λλ6716, 6731, [Ni II] λ7378 and [Fe II] λ8617 intensities in column (3) of Table 1 suggest $N(\mathrm{Ni})/N(\mathrm{S}) = 7.6\, r_\odot$ and $N(\mathrm{Fe})/N(\mathrm{S}) = 0.1\, r_\odot$, where $r_\odot$ is the relevant solar abundance ratio (Allen 1973). Also, we note that the [C I] λλ9823, 9850 emission, compared with [S II], is about 7 times stronger than predicted by the models of HM.

Figures 7*b* and 8*b* show extracted one-dimensional spectra for the emission knot marked with a short arrow in Figures 3*c* and 4*c*, and columns (6) and (7) of Table 1 contain measured and reddening corrected line intensities. This location is within the yellow/green area in Figure 3 of UM, which characterizes most of the filamentary structure. The implied N(He)/N(H), derived from Figure 1 of HM, is roughly 1.5 (~86% helium mass fraction). We also derive $N(\mathrm{Ni})/N(\mathrm{S}) = 4.9\, r_\odot$ and $N(\mathrm{Fe})/N(\mathrm{S}) = 0.08\, r_\odot$.

For the LHeR position which is marked with a long arrow in Figures 3*c* and 4*c*, one-dimensional spectra are illustrated in Figures 7*c* and 8*c*, while relative measured and reddening corrected line intensities are listed in columns (8) and (9) of Table 1. The data yield $N(\mathrm{He})/N(\mathrm{H}) = 0.16$, $N(\mathrm{Ni})/N(\mathrm{S}) = 54\, r_\odot$, and $N(\mathrm{Fe})/N(\mathrm{S}) = 0.82\, r_\odot$, with [C I] λλ9823, 9850/[S II] λλ6716, 6731 again being about 7 times greater than predicted by the HM models.

Whereas measured lines may imply high nickel abundances in a variety of phenomena, including other supernova remnants, some Seyfert galaxies, the Orion Nebula, and some Herbig-Haro objects (see Henry and Fesen 1988), the Crab Nebula's northern arch structure appears to be the most extreme case by far. In an effort to determine the maximum nickel line enhancement and to investigate a possible cause for such strong emission, we obtained the spectrum of Figure 5 with the slit running across the arch. A one-dimensional extraction at the location marked with an arrow is illustrated in Figure 10, and line measurements may be found in columns (10) and (11) of Table 1. The [S II] λλ6716/6731 ratio yields an electron density of about 10^3 cm^{-3}, while the [Ni II] λλ7411/7378 ratio of 0.06 suggests an electron temperature near 5000 K (see Henry 1987). The latter is reasonably consistent with a temperature of order 10,000 K derived from [O III] lines (see HM). We derive a maximum $N(\mathrm{Ni})/N(\mathrm{S}) = 55\, r_\odot$, which is similar to what we found above. The most interesting new aspect of Figure 5 is the sharply discontinuous velocity structure for filaments near the position of star D, or just beyond the western edge of the arch. The central arch emission has a measured velocity of order +500 km s^{-1}, compared with about +1100 km s^{-1} for emission in the filament just to the west of star D. This may be evidence for an ambient cloud interacting with (and impeding) some moderately high-velocity ejecta, a point which is relevant to the discussion below.

Enormous spatial variations exist in the deduced helium, nickel, and iron abundances. The measurements presented in Table 1 do not support the suggestion, made above from examination of the two-dimensional spectra, that anomalously strong [C I] λλ9823, 9850 is confined primarily to the HHeB; but the data do confirm that exceptionally strong [Ni II] emission arises in the LHeR. In addition, we note that the [Ni II] λ7378/[Fe II] λ8617 ratio does not vary greatly among the different positions considered. We do not know with certainty that the [C I], [Ni II], and [Fe II] lines are produced by thermal electron collisional excitation, as assumed in the abundance calculations. Alternative mechanisms and a variety of possible implications have been considered by Henry, MacAlpine, and Kirshner (1984) and Henry and Fesen (1988). However, because a number of different line intensities are involved and derived gas conditions (temperature and density) do not appear to be substantially discrepant in the different regions of origin, actual abundance anomalies seem at least as plausible as unusual physical processes which target specific atomic transitions in certain filament locations.

For the LHeR, a helium/hydrogen ratio which is significantly lower than average along with abnormally high nickel and iron abundances may be related in a consistent fashion with formation of the jetlike structure in this part of the nebula. Morrison and Roberts (1985) postulated that the jet resulted from interaction of supernova ejecta with an ambient interstellar cloud, and, as noted above, the discontinuous velocity structure in Figure 5 may be direct evidence for this. The relatively low helium mass fraction could be due to a preponderance of hydrogen-rich cloud material. Also, in reference to SN 1987A, Woosley (1988) has pointed out that nickel-rich material explosively produced in the central region of the supernova may, for the right conditions, be Rayleigh-Taylor unstable at the interface with the overlying helium-rich mantel. In the Crab Nebula, increased density contrast involving ejected material and the postulated interstellar cloud could have caused this kind of mixing and resultant nickel enrichment in the LHeR. Then, assuming there was ^{58}Ni along with unstable ^{56}Ni, it could show up today primarily in the LHeR because of its concentration and the relatively high emission measure there compared with other ^{58}Ni containing gas. If this

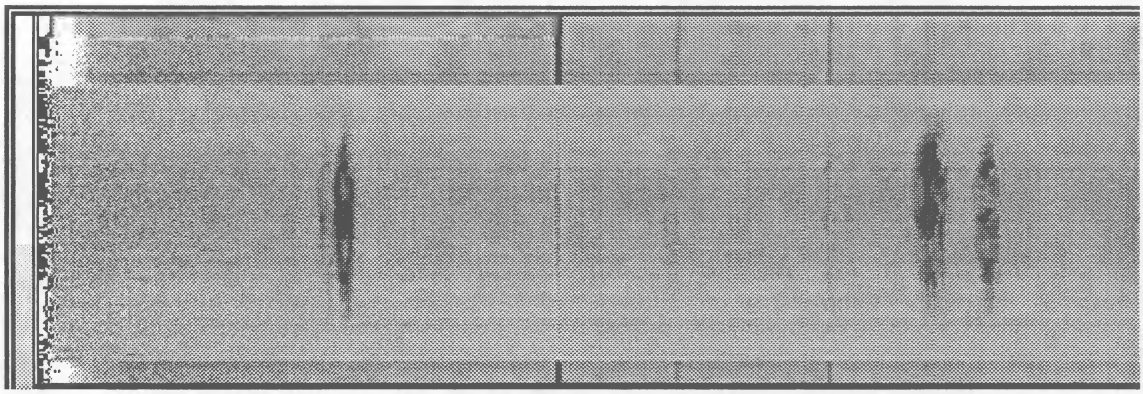

FIG. 11.—Long-slit (north-south orientation) two-dimensional drift scan for the Crab Nebula as a whole. The approximate wavelength range is 4300 Å–7200 Å. Line identifications may be found in Fig. 12.

is correct, the ratio of ^{58}Ni to ^{56}Fe (the ultimate decay product of ^{56}Ni), which appears relatively constant for different positions in our data, may reflect the neutron richness of the environment which existed in the core of SN 1054. Also, if the apparent nickel enhancement is localized and results from an extraneous factor, an ambient cloud, then the stigma whereby SN 1054 must have been "one of a kind" by producing far too much nickel may not be such a problem.

IV. RELATIVE LINE INTENSITIES AND CHARACTERISTICS FOR THE NEBULA AS A WHOLE

On 1987 October 15/16, the McGraw-Hill 1.3 m telescope was used with the Mark III spectrograph and the Thomson CCD to obtain long-slit "drift scans" across the nebula as a whole. The north-south slit, with projected dimensions of 2.″3 × 9′, was repeatedly driven smoothly across the nebula at a rate of about 90 seconds of arc per minute of time. The starting and ending points of each additive scan were chosen to lie just outside the maximum extent of the [O III] emission region illustrated by Gull and Fesen (1982).

The fully reduced two-dimensional spectrum is shown in Figure 11. The velocity ellipse for [O III] λ5007 appears somewhat wasp-waisted, implying that the bipolar structure reported above may reflect to some extent the global properties of the nebula.

The one-dimensional integrated spectrum is presented in Figure 12. Relative line intensities are similar to those reported by Davidson (1987) (except we were unable to measure He II λ4686). We find a reddening corrected I(He I λ5876)/I(Hβ) of 0.7 ± 0.1 (excluding the poorly subtracted Na I λ5890 sky emission). Extrapolation of Figure 1 in HM for the relation between this ratio and N(He)/N(H) implies a value near 3 for

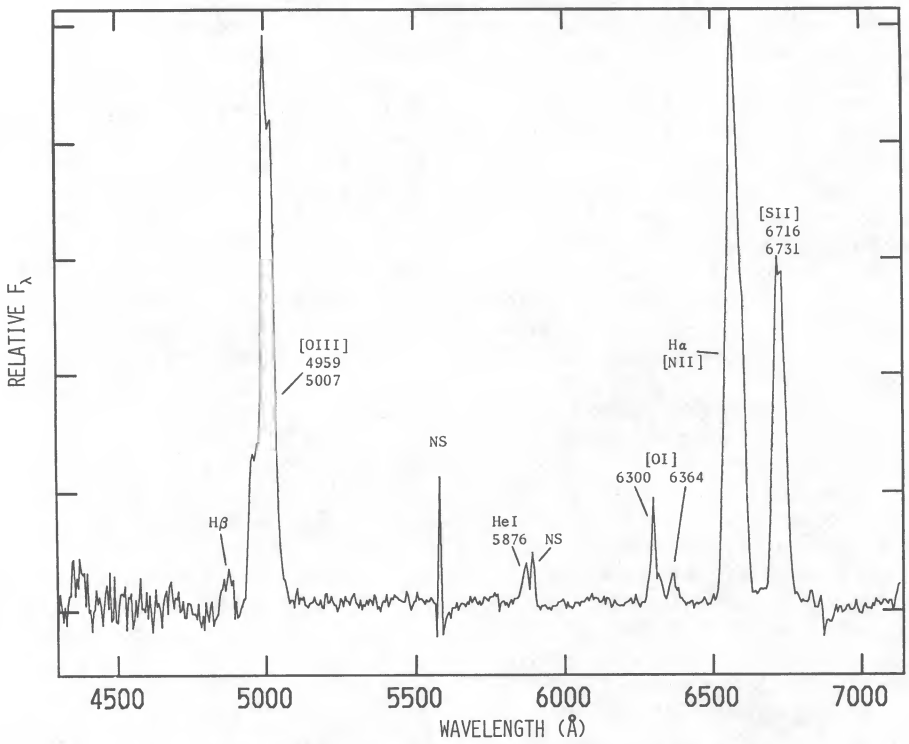

FIG. 12.—Integrated spectrum for the Crab Nebula as a whole, taken from Fig. 11

the latter. Then, a nebular hydrogen mass of 0.45 $M_\odot$, as estimated by HM, would suggest a total hydrogen plus helium mass around 6 $M_\odot$. If we consider some fraction, for example 25%, of the Hβ emission as coming from interstellar cloud gas (in the LHeR) with I(He I λ5876) = 0.2 I(Hβ) (see Table 1 entries for the LHeR), the estimated hydrogen mass (mostly H^0) of remnant gas would drop to 0.40 $M_\odot$, for which I(He I λ5876)/I(Hβ) $\approx$ 0.87. Then the overall deduced mass of emitting nebular material would *increase* to perhaps 7 $M_\odot$ or more. Furthermore, the global I(He II λ4686)/I(Hβ) measured by Davidson is roughly twice what HM predicted for plane-parallel filament models, supporting the idea that the filaments are surrounded by high-ionization regions. That being the case, there would be still more helium contributing to the filamentary mass than accounted for in the HM calculations. If the progenitor object that exploded contained 9–10 $M_\odot$, as suggested by Nomoto (1985), then most of it may be visible in the nebular gas and neutron star. This would alleviate the problem of accounting for 6 $M_\odot$ of material previously postulated as existing in a rapidly expanding, undetected circumnebular shell (see § I). However, it would also suggest there was considerably more mass associated initially with the progenitor, which (by analogy with SN 1987A) may have started out with 20–30 $M_\odot$ to have formed a 6–9 $M_\odot$ helium core. Very massive stars located 200 pc or more from the galactic plane are not unheard of (see, e.g., Nichols-Bohlin and Fesen 1986) and could, in some cases, have gotten there as runaway objects lost from a cluster or a binary system (see, e.g., Conti, Leep, and Lorre 1977; Moffat and Seggewiss 1979). For the Crab Nebula in particular, a runaway star hypothesis has previously been espoused by Gott, Gunn, and Ostriker (1970) and by Minkowski (1970), partly to account for the pulsar's high observed space velocity.

Because the above nebular mass estimates are significantly higher than those derived previously and because of resultant implications for the nature of the precursor star, it is appropriate that we briefly review the calculative procedures and uncertainties. Whereas our emission-line data for the Crab Nebula as a whole do not differ greatly from earlier measurements, a major consideration is the dependence of I(He I λ5876)/I(Hβ) on N(He)/N(H), as modeled by HM. This is a primary cause for revised estimates of the overall helium mass compared with that of hydrogen. The latter was estimated by HM from the total Hβ line intensity (for the H^+ fraction) and from the total [S II] $\lambda\lambda$6716, 6731 intensity (for the H^0 fraction). The relevant calculations involve assumptions about the gas density and temperature as well as N(S)/N(H). Reasonable values, based on observational measurements and photoionization models, were adopted for these quantities; but the ranges of uncertainty when applied to the nebula as a whole are noteworthy. Considering all the above factors, *any* nebular mass estimate must be considered with caution. Nevertheless, it is appropriate that we point out possible implications of plausibly high nebular mass, as discussed above.

Finally, we note that the [O III] $\lambda\lambda$4959, 5007 emission equivalent width measured from our drift scan is $\sim$280 Å (with no correction for continuum contributed by stars), which is similar to the equivalent width reported by Davidson (1987) but considerably higher than cited by O'Dell (1962), Kirshner (1974), or Davidson, Crane, and Chincarini (1974). Davidson suggested that the apparently increasing line equivalent width may result from rapidly decreasing continuum flux in the nebula (but see also Veron-Cetty and Woltjer 1988).

V. SUMMARY

Observations presented here and in UM suggest that much of the brighter filamentary gas in the Crab Nebula is involved in large structures consisting of a nearly pure helium band or torus and bipolar, helium-rich lobes. Long-slit spectra confirm exceptionally strong He I emission, which is confined to a patchy east-west strip in the vicinity of the neutron star. The measured relative line intensities indicate that collisional contributions to the observed helium lines are insignificant, so the use of I(He I λ5876)/I(Hβ) to derive N(He)/N(H) is valid, and locations with $\sim$95% helium by mass are found. In addition, for north-south slit orientations, the two-dimensional spectra show emission-line velocity ellipses which have a central pinched appearance, as if the nebular expansion were constrained in the vicinity of the helium band or torus. This is consistent with the existence of north-south lobes, as suggested by Figure 3 of UM.

From our long-slit drift-scan spectrum for the Crab Nebula as a whole and similar data reported by Davidson (1987), we used the model computation results of HM to estimate a combined mass of emitting gas (primarily helium) and the neutron star, which may be as high as 6–9 $M_\odot$. Such a large helium core may indicate that the supernova precursor initially contained 20–30 $M_\odot$ while on the main sequence. Also, our measured [O III] $\lambda\lambda$4959, 5007 equivalent width for the entire nebula agrees with Davidson's recently reported value and is substantially larger than measurements cited 14 and 26 years ago.

Images through interference filters and spectroscopy confirm large spatial variations in the [Ni II] λ7378 line intensity relative to [S II] $\lambda\lambda$6716, 6731. The [Ni II] λ7378 line *suggests* an abundance enhancement by a factor of about 55 compared with solar in the northern arch-shaped structure. In general, the strongest [Ni II] emission coincides with regions of relatively low helium abundance in the northeast part of the nebula, near the base of the jetlike protrusion. The apparently discontinuous velocity structure in one of our spectra is consistent with the idea that this overall situation may have resulted from interaction between an ambient interstellar cloud and material produced in the supernova core, including nickel-rich gas normally associated with radioactivity during the late stages of outburst. We find the [Ni II] λ7378/[Fe II] λ8617 ratio to be large and relatively constant spatially, possibly indicative of a neutron-rich explosive environment during production of iron peak elements. Alternatively, the deduced $N(^{58}Ni^+)/N(^{56}Fe^+)$ of order 60–75 times the solar value could result from the relatively young age of the Crab Nebula, for which some key inferences involving straightforward equilibrium photoionization model calculations may not be applicable. We are presently looking into this question, which could also have implications for derived $N(Ni^+)/N(S^+)$ values.

We acknowledge informative conversations with W. Blair, K. Davidson, C. Cowley, R. Fesen, M. Gaskell, P. Hughes, G. Kriss, K. Long, P. Morrison, R. Sears, and J. Truran. This work was partially supported by the National Science Foundation.

REFERENCES

Allen, C. W. 1973, *Astrophysical Quantities* (3d ed.; London: Athlone), p. 31.
Berrington, K. A., Burke, P. G., Freitas, L. C. G., and Kingston, A. E. 1985, *J. Phys. B*, **18**, 4135.
Berrington, K. A., and Kingston, A. E. 1987, *J. Phys. B*, **20**, 6631.
Clark, D. H., Murdin, P., Wood, R., Gilmozzi, R., Danziger, J., and Furr, A. W. 1983, *M.N.R.A.S.*, **204**, 415.
Clegg, R. E. S. 1987, *M.N.R.A.S.*, **229**, 31P.
Conti, P. S., Leep, E. M., and Lorre, J. J. 1977, *Ap. J.*, **214**, 759.
Davidson, K. 1973, *Ap. J.*, **186**, 223.
———. 1978, *Ap. J.*, **220**, 177.
———. 1979, *Ap. J.*, **228**, 179.
———. 1987, *A.J.*, **94**, 964.
Davidson, K., Crane, P., and Chincarini, G. 1974, *A.J.*, **79**, 791.
Davidson, K., and Fesen, R. A. 1985, *Ann. Rev. Astr. Ap.*, **23**, 119.
Davidson, K., Gull, T. R., Maran, S. P., Stecher, T. P., Fesen, R. A., Parise, R. A., Harvel, C. A., Kafatos, M., and Trimble, V. L. 1982, *Ap. J.*, **253**, 696.
Dennefeld, M., and Andrillat, Y. 1981, *Astr. Ap.*, **103**, 44.
Dennefeld, M., and Péquignot, D. 1983, *Astr. Ap.*, **127**, 42.
Eastman, R. G., MacAlpine, G. M., Kirshner, R. P., and Henry, R. B. C. 1985, in *The Crab Nebula and Related Supernova Remnants*, ed. M. Kafatos and R. B. C. Henry (Cambridge: Cambridge University Press), p. 19.
Feldman, F. R., and MacAlpine, G. M. 1978, *Ap. J.*, **221**, 486.
Ferland, G. J. 1986, *Ap. J. (Letters)*, **310**, L67.
Fesen, R. A., and Kirshner, R. P. 1982, *Ap. J.*, **258**, 1.
Flannery, M. R., and McCann, K. J. 1975, *Phys. Rev. A*, **12**, 846.
Gott, J. R., Gunn, J. E., and Ostriker, J. P. 1970, *Ap. J. (Letters)*, **160**, L91.
Gull, T. R., and Fesen, R. A. 1982, *Ap. J. (Letters)*, **260**, L75.
Henry, R. B. C. 1986, *Pub. A.S.P.*, **98**, 1044.
———. 1987, *Ap. J.*, **322**, 399.
Henry, R. B. C., and Fesen, R. A. 1988, *Ap. J.*, **329**, 693.
Henry, R. B. C., and MacAlpine, G. M. 1982, *Ap. J.*, **258**, 11 (HM).
Henry, R. B. C., MacAlpine, G. M., and Kirshner, R. P. 1984, *Ap. J.*, **278**, 619.
Kirshner, R. P. 1974, *Ap. J.*, **194**, 323.
MacAlpine, G. M. 1976, *Ap. J.*, **204**, 694.
Mayall, N. U. 1937, *Pub. A.S.P.*, **49**, 101.
Miller, J. S. 1978, *Ap. J.*, **220**, 490.
Minkowski, R. 1942, *Ap. J.*, **96**, 199.
———. 1970, *Pub. A.S.P.*, **82**, 470.
Moffat, A. F. J., and Seggewiss, W. 1979, *Astr. Ap.*, **77**, 128.
Morrison, P., and Roberts, D. 1985, *Nature*, **313**, 661.
Murdin, P. G., and Clark, D. H. 1981, *Nature*, **294**, 543.
Nichols-Bohlin, J., and Fesen, R. A. 1986, *A.J.*, **92**, 642.
Nomoto, K. 1985, in *The Crab Nebula and Related Supernova Remnants*, ed. M. Kafatos and R. B. C. Henry (Cambridge: Cambridge University Press), p. 97.
O'Dell, C. R. 1962, *Ap. J.*, **136**, 809.
Osterbrock, D. E. 1974, *Astrophysics of Gaseous Nebulae* (San Francisco: Freeman), p. 71.
Péquignot, D., and Dennefeld, M. 1983, *Astr. Ap.*, **120**, 249.
Schattenberg, M. L., Canizares, C. R., Berg, C. J., Clark, G. W., Markert, T. H., and Winkler, P. F. 1980, *Ap. J. (Letters)*, **241**, L151.
Uomoto, A., and MacAlpine, G. M. 1987, *A.J.*, **93**, 1511 (UM).
Uomoto, A., MacAlpine, G. M., and Henry, R. B. C. 1985, in *The Crab Nebula and Related Supernova Remnants*, ed. M. Kafatos and R. B. C. Henry (Cambridge: Cambridge University Press), p. 9.
van den Bergh, S. 1970, *Ap. J. (Letters)*, **160**, L27.
Velusamy, T. 1985, in *The Crab Nebula and Related Supernova Remnants*, ed. M. Kafatos and R. B. C. Henry (Cambridge: Cambridge University Press), p. 115.
Veron-Cetty, M.-P., and Woltjer, L. 1988, *Astr. Ap.*, **201**, L27.
Williams, R. E. 1967, *Ap. J.*, **147**, 556.
Wilson, A. S., and Weiler, K. W. 1982, *Nature*, **300**, 155.
Woltjer, L. 1958, *Bull. Astr. Inst. Netherlands*, **14**, 39.
Woosley, S. E. 1988, in *IAU Colloquium 108, Atmospheric Diagnostics of Stellar Evolution*, ed. K. Nomoto, in press.

GORDON M. MACALPINE, JOSEPH M. MAZZARELLA, and STACY S. MCGAUGH: Department of Astronomy, University of Michigan, Ann Arbor, MI 48109

ALAN UOMOTO: Department of Physics and Astronomy, Johns Hopkins University, Baltimore, MD 21218